Distribution Agreement

In presenting this thesis as a partial fulfillment of the requirements for a degree from Emory University, I hereby grant to Emory University and its agents the non-exclusive license to archive, make accessible, and display my thesis in whole or in part in all forms of media, now or hereafter now, including display on the World Wide Web. I understand that I may select some access restrictions as part of the online submission of this thesis. I retain all ownership rights to the copyright of the thesis. I also retain the right to use in future works (such as articles or books) all or part of this thesis.

Yifeng Shi April 10, 2024

Unraveling the Mobilization and Interplay of Immune Cells in Rodent Hepacivirus Infection

by

Yifeng Shi

Dr. Arash Grakoui
Adviser

Department of Biology

Dr. Arash Grakoui

Adviser

Dr. Manoj Thapa

Committee Member

Dr. Dieter Jaeger

Committee Member

2024

Unraveling the Mobilization and Interplay of Immune Cells in Rodent Hepacivirus Infection

By

Yifeng Shi

Dr. Arash Grakoui

Adviser

An abstract of
a thesis submitted to the Faculty of Emory College of Arts and Sciences
of Emory University in partial fulfillment
of the requirements of the degree of
Bachelor of Science with Honors

Department of Biology

2024

Abstract

Unraveling the Mobilization and Interplay of Immune Cells in Rodent Hepacivirus Infection

By Yifeng Shi

Hepatitis C virus (HCV), a bloodborne pathogen known for causing liver inflammation and damage, presents a significant challenge to global health, particularly in the absence of a vaccine. This research delved into the study of rodent hepacivirus (RHV), a rodent analog of HCV, to unravel the complexities of HCV's pathogenesis. Utilizing KiKGR ROSA26 knock-in mice, capable of fluorescent cell labeling, we meticulously monitored the movements and behaviors of various immune cells during the course of infection. With a focus on the spleen as a crucial secondary lymphoid organ, we examined its role and subsequent effects on the liver post-infection (p.i.). Our findings revealed a plausible early infection influx of splenic innate cells and an accumulation of liver-resident monocytes (day 3 p.i.), followed by a heightened innate immune response characterized by a rise in liver-resident macrophages (day 7 p.i.), and later, an infiltration of splenic T cells and B cells, leading to an enhanced presence of $CD8^+$ effector and memory cells in the liver (days 12 p.i.). Further insights from CCR2 knock-out mice indicated that $CCR2^+$ monocytes/macrophages were not crucial in the virus' progression and clearance. This investigation enriched our understanding of immune responses in RHV infection and laid down a valuable groundwork for HCV research, potentially influencing future therapeutic strategies and vaccine development against viral diseases.

Unraveling the Mobilization and Interplay of Immune Cells in Rodent Hepacivirus Infection

By

Yifeng Shi

Dr. Arash Grakoui

Adviser

A thesis submitted to the Faculty of Emory College of Arts and Sciences
of Emory University in partial fulfillment
of the requirements of the degree of
Bachelor of Science with Honors

Department of Biology

2024

Acknowledgements

I would like to express my special thanks of gratitude to my advisor, Dr. Arash Grakoui, for providing me with lab resources to conduct my study. I also want to thank Dr. Manoj Thapa for being a wonderful mentor, and Dr. Anuradha Kumari for assisting with my experiments.

Secondly, I am thankful to Animal Care staff and Veterinary staff of Emory Primate Research Center for assistance during the study.

Table of Contents

1. INTRODUCTION

Hepatitis C virus (HCV) is a global prevalent pathogen recognized as a leading cause of liver diseases, including cirrhosis, hepatocellular carcinoma, and liver cancer (Chen & Morgan, 2006). It is primarily transmitted through exposure to infected blood, with high-risk activities like intravenous drug injection and non-sterile medical procedures being the leading causes of the spread (Alter, 2007). Though recent advancements in antiviral therapy, particularly the development of direct-acting antivirals (DAAs), have treated infected individuals, eradicating the virus requires an effective vaccine (Hayes et al., 2022).

The development of HCV vaccine is mainly hindered by a lack of small animal models since HCV does not cause a persistent infection in small animals. In New York City, a close relative of HCV, rodent hepacivirus (RHV), was discovered in feral rats (Atcheson et al., 2020). According to Kapoor et al., the two viruses' genomes both possess long 5' untranslated regions (UTRs) with internal ribosome entry site (IRES) elements, which are important for the viruses' translation mechanisms, and a miR-122 binding site, which is functionally required for HCV replication in hepatocytes. Additionally, RHV's 3' UTR shares structural elements with HCV's, including a variable region following the open reading frame (ORF), a polypyrimidine tract, and a 3' X region (Kapoor et al., 2013). Therefore, due to their genomic structure similarities, RHV has served as a potential surrogate model of human HCV to study its pathogenesis in small animal models.

Upon viral invasion, a host's immune defenses are activated, encompassing the innate and adaptive systems. The innate immune system rapidly mobilizes to impede the initial stages of infection indiscriminately. Its cellular arsenal, consisting of monocytes, macrophages, dendritic cells, neutrophils, and natural killer cells, performs critical tasks such as pathogen phagocytosis

and the secretion of interferons and pro-inflammatory cytokines. In juxtaposition, the adaptive immune system, while slower to react initially, offers durable immunity. It leverages B cells and T cells, which are integral in producing antibodies that specifically target and neutralize viral entities, and directly killing infected cells (Mueller et al., 2008).

Past investigations of RHV infection in mice showed that RHV induced the expansion of immune cells, particularly $CD8^+$ and $CD4^+$ T cells, in mice (Billerbeck et al., 2017), and that $CD8^+$ T cells were more enriched in the liver than in the spleen (Hartlage et al., 2019). However, it is not known whether these immune cells were primed in the liver or in the secondary lymphoid organs before migrating to the liver. Previous studies trying to decipher the activating roles of monocytes and macrophages in HCV and hepatitis B virus (HBV) showed that the uptake of virus by the cells triggered the release of pro-inflammatory and anti-inflammatory mediators that resulted in the activation of natural killer (NK) cells and $CD8^+$ T cells, blockage of viral replication, and attraction and activation of innate lymphoid cells (ILCs), plasmacytoid dendritic cells (pDCs), and regulatory T cells (Tregs) (Li & Tu, 2017). Therefore, understanding the initiation of innate response that facilitates the establishment of adaptive immunity may offer a comprehensive view of the kinetics of RHV. Taken together, we are intrigued by the migration pattern of $CD8^+$ T cells, monocytes, and macrophages during RHV infection and understanding this migration pattern is the main focus of our study.

Moreover, detailed interactions between immune cells remain poorly documented. A previous study showed that RHV immunity was indeed established by the cooperation of different immune cells, and specifically, CD4+ T cells helped the development of CD8+ T cells, and without CD4+ T cells, RHV escape variants targeted CD8+ T cells and can subvert immunity

(Hartlage et al. 2019). Thus, it is important to study how immune cells interact during an infection, and this knowledge will be useful in the development of vaccine. Perhaps, boosting immune cells that CD8+ and CD4+ T cells rely on will improve the overall immunity.

Since the control of HCV infection depends heavily on the generation and maintenance of an effective T cell immunity, therefore in this study, we aim to monitor the migration of T cells and B cells as well as that of monocytes and macrophages which contribute to T cells and B cells maturation during an acute RHV infection; we also aim to investigate how different types of immune cells interact.

In this study, the spleen is identified as the key launch site for the movement of immune cells, given its vital role as a secondary lymphoid organ. It hosts a variety of immune cells, such as macrophages, which engulf viruses and present their antigens to T cells, and B cells, which mature into plasma cells and produce viral-specific antibodies. Additionally, the spleen facilitates the interaction among immune cells, thereby reinforcing the body's immune responses (Bronte & Pittet, 2013). Therefore, we focused on tracing the pathways of these immune cells as they travel from the spleen to the site of infection, the liver.

For our experimental approach, we measured the relative frequencies and the kinetics of immune cells, mainly T cells, B cells, monocytes, and macrophages, in the liver during an acute infection. We infected mice with 10^4 genomic equivalent (GE) units of RHV, and spleen was fluorescently labelled and harvested with liver at day 3, 7, and 12 post infection to analyze the longitudinal migration of these cells. We expect our results will define the immune correlates needed to prevent chronic RHV infection.

2. MATERIALS AND METHODS

1. KiKGR ROSA26 Knock-in Mice

In this study, we utilized a transgenic KiKGR ROSA26 knock-in mice that express a photoconvertible fluorescence protein in all cells in the body, which, upon exposure to 403 nm LED light, changes color from green to red. This mouse model will be useful to investigate the kinetics of immune cells (B cells, T cells, monocytes, macrophages, and etc.) migration during an acute RHV infection.

2. Experiment 1

KiKGR ROSA26 knock-in mice were selected and divided into four groups (n=5 mice/group): Group 1: mice infected with RHV and subjected to 403 nm LED light exposure on the spleen (RHV+LED+), Group 2: mice infected with RHV without 403 nm LED light exposure on the spleen (RHV+LED-), Group 3: mice without infection but subjected to 403 nm LED light exposure on the spleen (RHV-LED+), and Group 4: mice without infection or 403 nm LED light exposure on the spleen (RHV-LED-/controls). The mice in the RHV+ groups were infected via intravenous injection of 10^4 GE RHV, a procedure assisted by Dr. Anuradha Kumari. A subcostal laparotomy was performed, by Dr. Anuradha Kumari, on the mice in the LED+ groups, two days prior to the day of harvest, to allow the spleen of the mice to be exposed to 403 nm LED light of intensity 120 mW/cm^2 for 9 minutes (3 minutes on each of 3 distinct surfaces of the spleen to maximize cell conversion). The sugery was performed strictly two days prior to the day of harvest since the converted cells might lose fluorescence upon proliferation. Spleen and liver tissues were harvested at day 3, 7, and 12 post infection, followed by cell isolation and quantification. Serum

samples were collected for RNA extraction and quantification to determine the viral load. The longitudinal migration of red-labeled cells from the spleen to the liver was analyzed using flow cytometry, which measures the amount of green and red fluorescence emitted by cells in the spleen and liver. The composition (types of cells migrating) of the red-labeled cells in the infected livers were determined using specific surface markers staining and flow cytometry. Further investigation was conducted to assess the phenotypes and functions of these red-labeled cells in the liver.

3. Experiment 1 Techniques: Staining & Flow Cytometry

Following tissue preparation, liver cells, including the unconverted green cells and possibly the converted red cells, were stained with different color fluorescent antibodies targeting specific antigens. These antibodies directly bound to their respective antigens on the cell surfaces, enabling the accurate identification of unique cell groups based on the presence of these antigens. It's crucial to highlight that PE (red) and FITC (green) fluorescent tagged antibodies were avoided due to the unique properties of KiKGR ROSA26 knock-in mice, in which all unexposed cells appear green, and exposed cells turn red. After the application of these fluorescent markers, the stained cells were subjected to flow cytometric analysis. The flow cytometer works by detecting and measuring the fluorescence intensity emitted by each cell as it traverses a laser path, effectively quantifying the fluorescence. This method of fluorescence quantification allows the flow cytometer to precisely evaluate the levels of expression for the intended markers. Such in-depth analysis offers vital insights into the characteristics and functions of cells, significantly advancing our comprehension of intricate biological processes and systems.

4. CCR2 Knock-out Mice

Another mouse strain we employed was the CCR2 knock-out mice, which lack the CCR2 chemokine receptor crucial for recruiting and mobilizing monocytes and macrophages from secondary lymphoid organs (such as the spleen and bone marrow) to inflammatory sites. This impairment can compromise the immune response against various pathogens. Utilizing this mouse model would allow us to explore the potential involvement of splenic CCR2 monocytes and macrophages in the progression and clearance of RHV.

5. Experiment 2

Initial findings from Experiment 1 indicated that on days 3 and 7 following RHV infection, monocytes and macrophages migrated from the spleen to the liver. However, their significance in RHV progression and clearance remained uncertain. Since CCR2 is responsible for recruiting and mobilizing monocytes and macrophages from the spleen to the liver, we wanted to compare the viral load in CCR2 knock-out mice to that in wild-type mice during RHV infection. We hypothesized that if CCR2+ monocytes/macrophages played a role in RHV infection, the viral load in the blood would be different between infected CCR2 knock-out mice and the infected wild-type mice. To address this inquiry, five CCR2 knock-out mice and five wild-type mice were intravenously infected with 10^4 GE RHV, a procedure assisted by Dr. John Gridley. Weekly cheek blood samples were collected, by Dr. John Gridley, from the mice over a four-week period post-infection to quantify viral levels and ascertain disparities in disease progression and viral clearance between the two groups.

3. RESULTS

1. Day 3 Post Infection

On the third day p.i., the percentage of red cells in the liver was comparable between uninfected and infected mice. However, the total number of infiltrating lymphocytes in the liver of the infected mice were more than those of the uninfected mice, indicating that there were overall more red cells in the liver of the infected mice (**Figure 1**). Through antibody staining and flow cytometry, we discovered that these red cells consisted of cells from both innate and adaptive immune system (**Figure 2 and 3**).

Under innate immune system, the majority of red cells were neutrophils, followed by monocytes and dendritic cells. The mean percentages of these red subpopulations were consistently higher in the liver of the infected mice than those of the uninfected mice (**Figure 4**). However, the sample size was too small to infer a statistical difference. Surprisingly, few to no red macrophages and natural killer cells were detected in all liver samples (**Figure 2 and 3**).

Among all liver cells, the only cell type exhibiting a higher mean percentage in the infected group compared to the uninfected group was monocytes (**Figure 5**). Again, the sample size was too small to infer a statistical difference.

Under adaptive immune system, a relatively small amount of red B cells was traced, whose frequencies were similar across all liver samples according to the calculated averages. The rest of the red cells were mostly T cells, whose mean percentage was higher in the liver of the infected mice than that of the uninfected mice (**Figure 6**). Yet, the sample size was too small to infer a statistical difference. Further phenotyping of the red T cells revealed that only less than ten

percent of the population were $CD4^+$ helper T cells, consisting of comparable amounts of effector and naïve cells, while only less than one percent of all were $CD8^+$ cytotoxic T cells (**Figure 3**).

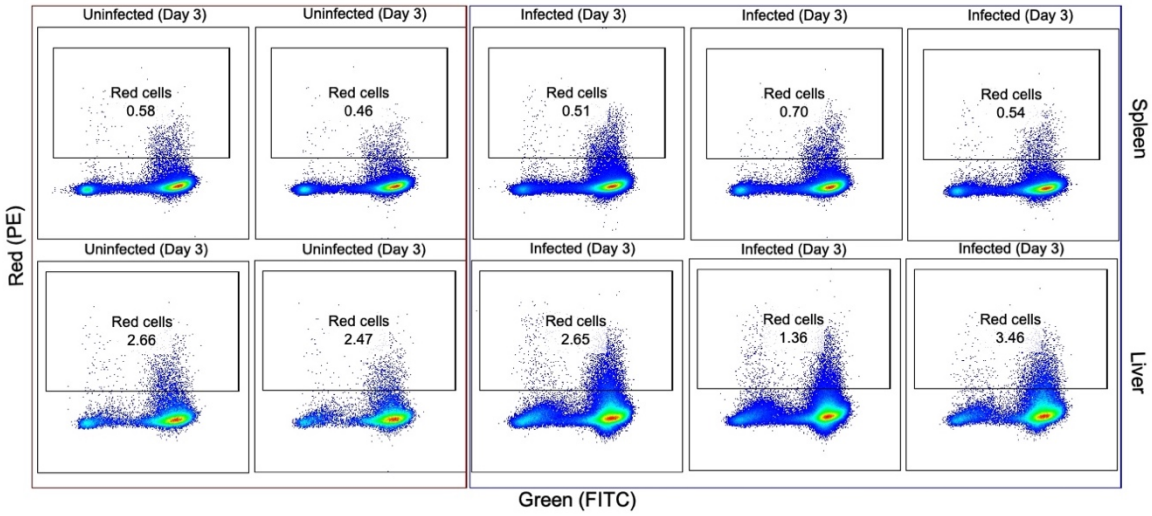

Figure 1

Percentage of red cells in the spleen and liver of uninfected vs. infected mice on day 3 p.i.

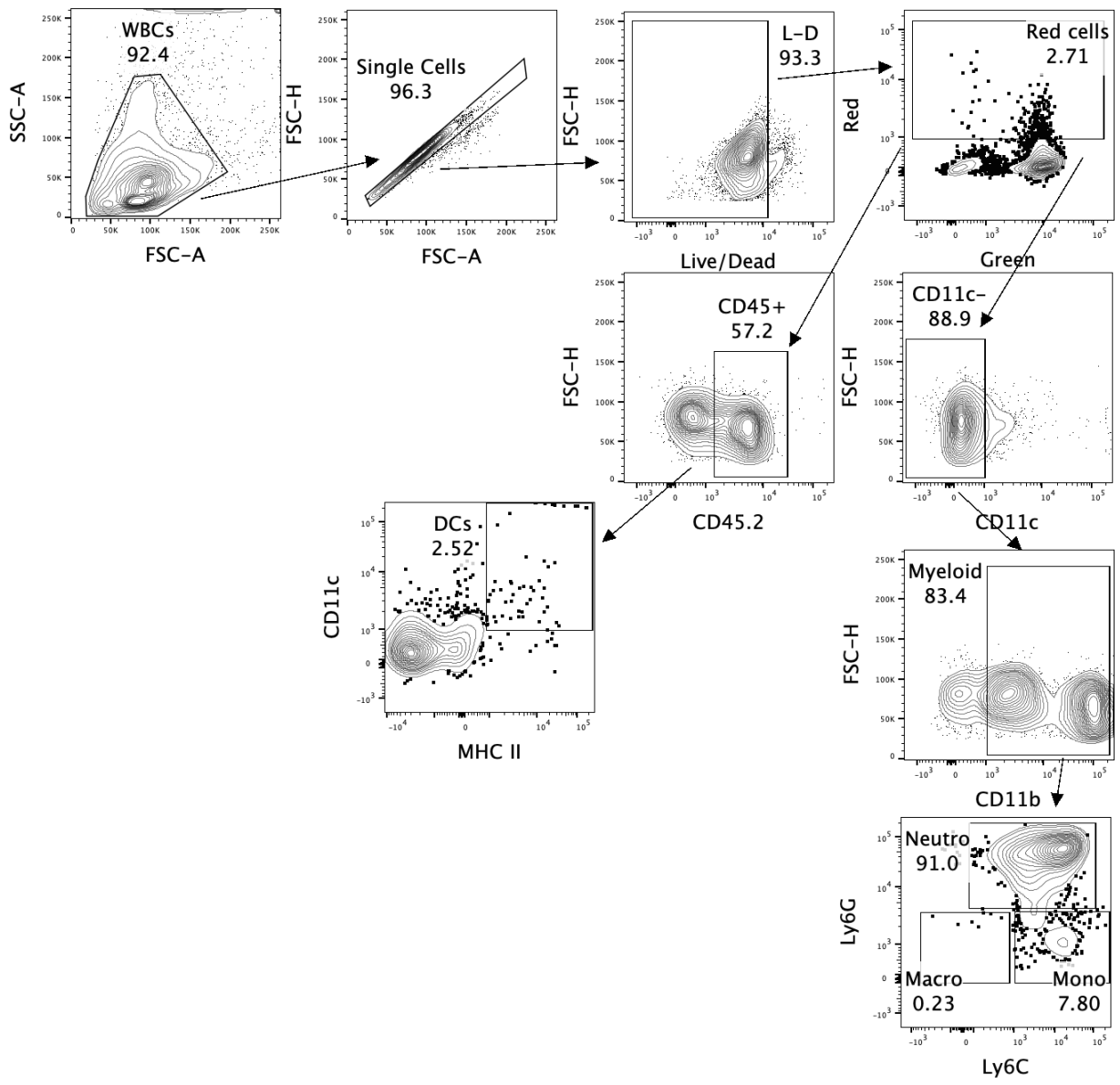

Figure 2

Flow cytometry gating scheme for mouse liver's innate immune cell populations on day 3 p.i. More concentrated circle = higher density of cells. The first plot (top left) identifies white blood cells (WBCs) based on their characteristic forward and side scatter, showing a 92.4% presence. Moving right, the next plot ensures that the sample contains single cells (96.3%) by comparing forward scatter width and height, which helps exclude cell aggregates. The third plot (top right) distinguishes live (93.3%) from dead based on their differential uptake of viability dyes or scatter profile. The last plot in the top row selects red cells (2.71%) based on their emitted red fluorescence. Moving down, the first plot in the second row shows CD45+ cells (57.2%), a common leukocyte marker, indicative of a general immune cell population. Following the arrow,

the next plot gates on CD11c+, MHC II+ cells (2.52%), which marks dendritic cells (DCs). The second plot in the second row excludes DCs by gating on CD11c- population (88.9%). Going down, the next plot displays myeloid cells (83.4%), identified by their expression of CD11b, and the final plot segregates neutrophils (91.0%), monocytes (7.80%), and macrophages (0.23%) based on the differential expression of Ly6C and Ly6G.

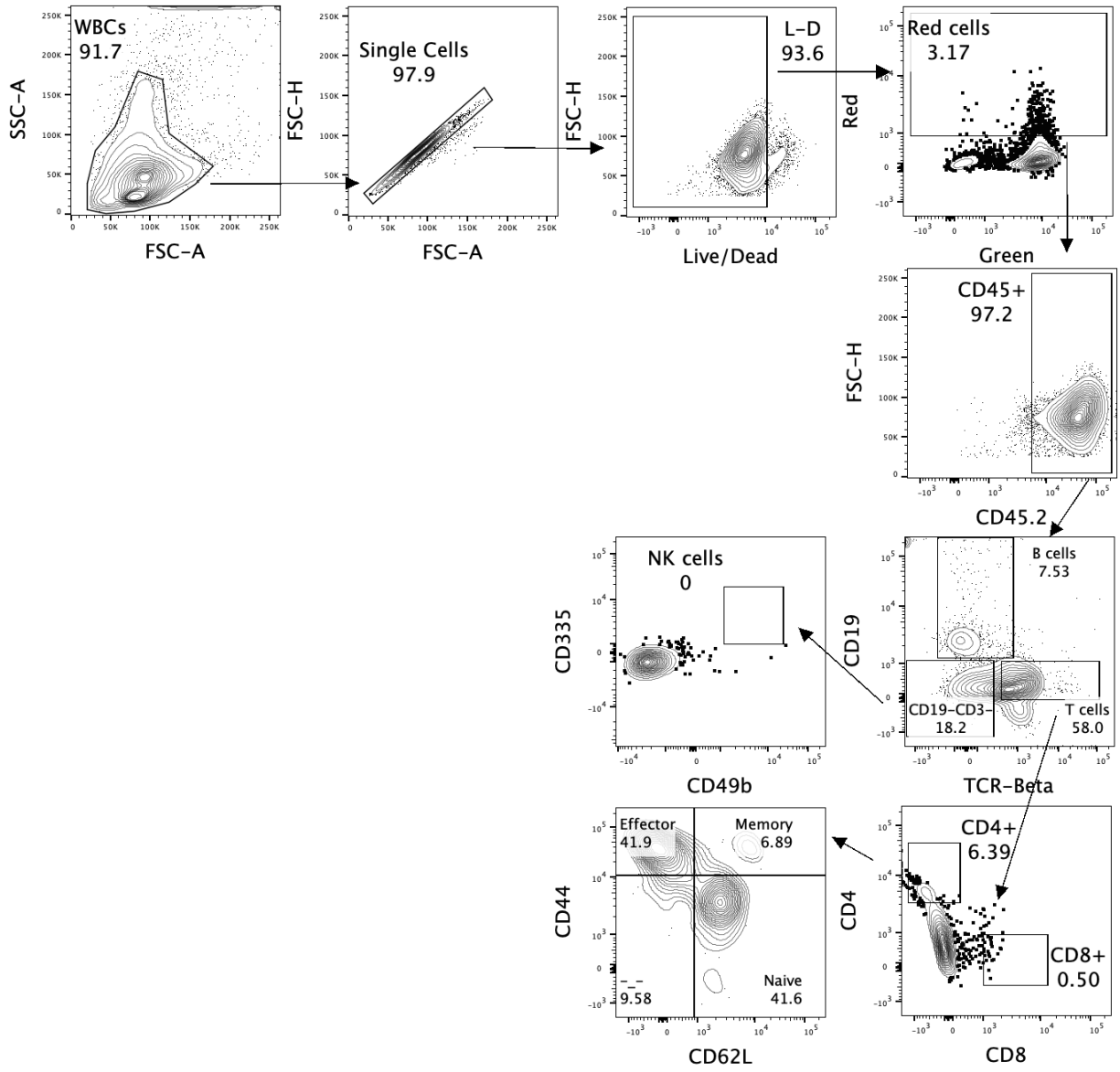

Figure 3

Flow cytometry gating scheme for mouse liver's adaptive immune cell populations on day 3 p.i. More concentrated circle = higher density of cells. The plots in the top row, like Figure 2, identify WBCs, single cells, live cells, and red cells, respectively. Going down from the red cells, the plot shows a nearly homogeneous population of CD45+ cells (97.2%), indicating that the vast majority of the cells in the sample are immune cells. Following the arrow, the next plot differentiates B

cells (7.53%) from T cells (58.0%) using CD19 and TCR-Beta markers, respectively. The population in absence of both markers is used to identify NK cells (0%), which express both CD335 and CD49b. Going down from the T cells, the plot distinguishes CD4+ helper T cells (6.39%) from CD8+ cytotoxic T cells (0.50%), both essential for orchestrating and executing immune responses. The CD4+ helper T cells are further characterized by the distribution of their subsets into naive (41.6%), memory (6.89%), and effector (41.9%) cells, which represent different stages of T cell activation and response.

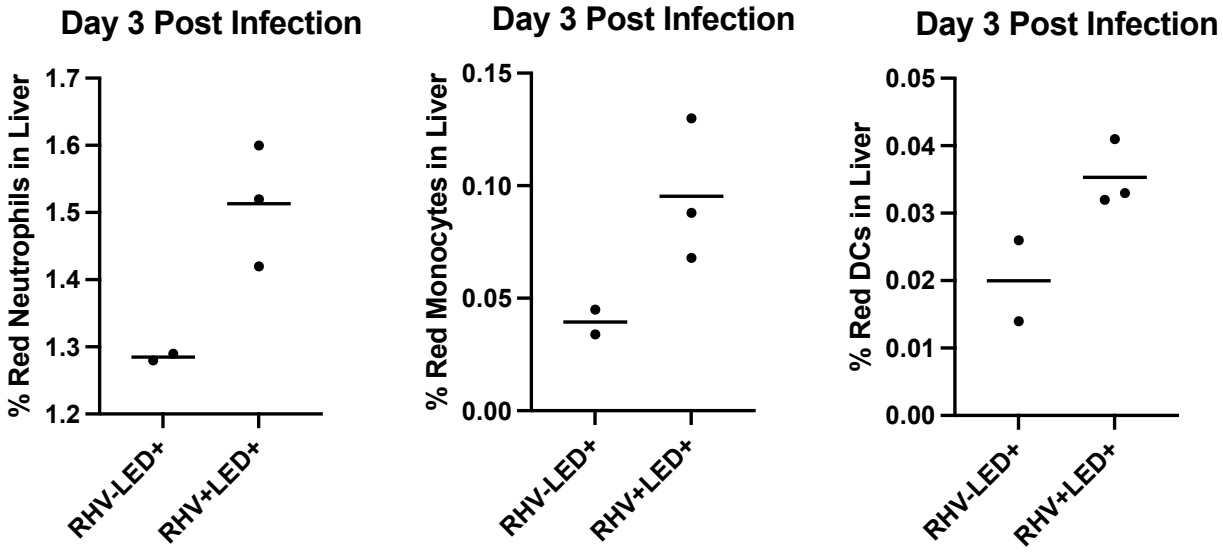

Figure 4

Percentage of red neutrophils, monocytes, and dendritic cells in the liver of infected vs. uninfected mice on day 3 p.i. (the horizontal bold lines represent the means)

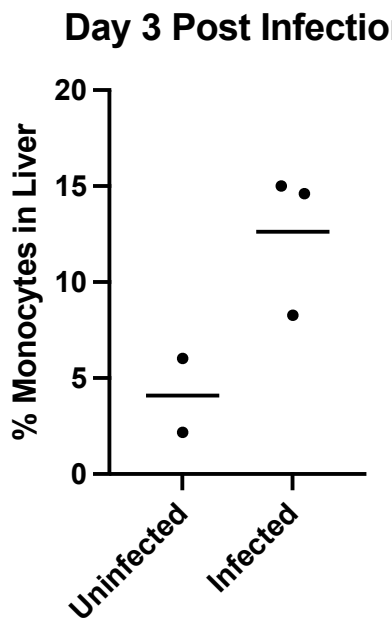

Figure 5

Percentage of liver-resident monocytes in the liver of infected vs. uninfected mice on day 3 p.i. (the horizontal bold lines represent the means)

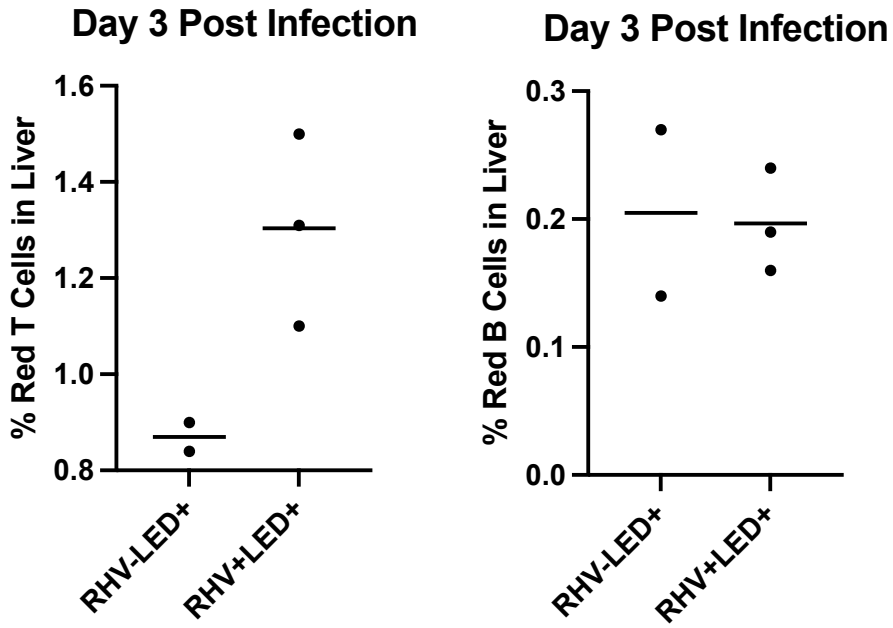

Figure 6

Percentage of red CD3 T cells and B cells in the liver of infected vs. uninfected mice on day 3 p.i. (the horizontal bold lines represent the means)

2. Day 7 Post Infection

On the seventh day p.i., we observed that more liver cells were isolated from the infected mice compared to the uninfected mice, indicated by the larger cell pellet. Utilizing the same methodology, the phenotypes of red cells in the liver were characterized, with the majority still stemming from the innate immunity (**Figure 7 and 8**). Notably, the percentage of red monocytes in the liver experienced a significant rise compared to day 3 p.i.. In the two surgical groups, the mean percentage of red monocytes was higher in the liver of the infected mice than that of the uninfected mice, though this disparity did not reach statistical significance. Unlike day 3 p.i., newly formed red macrophages were observed in the liver. However, their frequency in the liver did not significantly differ between the infected mice and the uninfected mice in the two surgical groups, as indicated by the overlapping confidence intervals, though the mean frequency might be slightly higher in the infected group (**Figure 9**).

Interestingly, in the two surgical groups, the mean percentage of red neutrophils was higher in the liver of the uninfected mice than that of the infected mice, though this difference was not statistically significant. This contradicted the trend observed on day 3 p.i.. It's worth noting that in the non-surgical groups, there was an abnormal presence of red cells in the liver for all three cell types (**Figure 9**). Same as day 3 p.i., no natural killer cells were captured.

Among all liver cells, the only cell type exhibiting a significantly higher percentage in the infected group compared to the uninfected group was macrophages, as indicated by the non-overlapping confidence intervals (**Figure 10**).

Concerning adaptive immunity, the percentages of red B cells and T cells in the liver remained low and were similar across all groups, irrespective of the irregular presence of red cells in the

final control group (**Figure 11**). Upon further phenotyping, the red T cells in the infected group exhibited nearly identical levels of $CD4^+$ and $CD8^+$ T cells, predominantly consisting of naïve cells (**Figure 8**). Similarly, the liver-resident T cells in the liver of the infected consisted of similar levels of $CD4^+$ and $CD8^+$ T cells, also predominantly consisting of naïve cells.

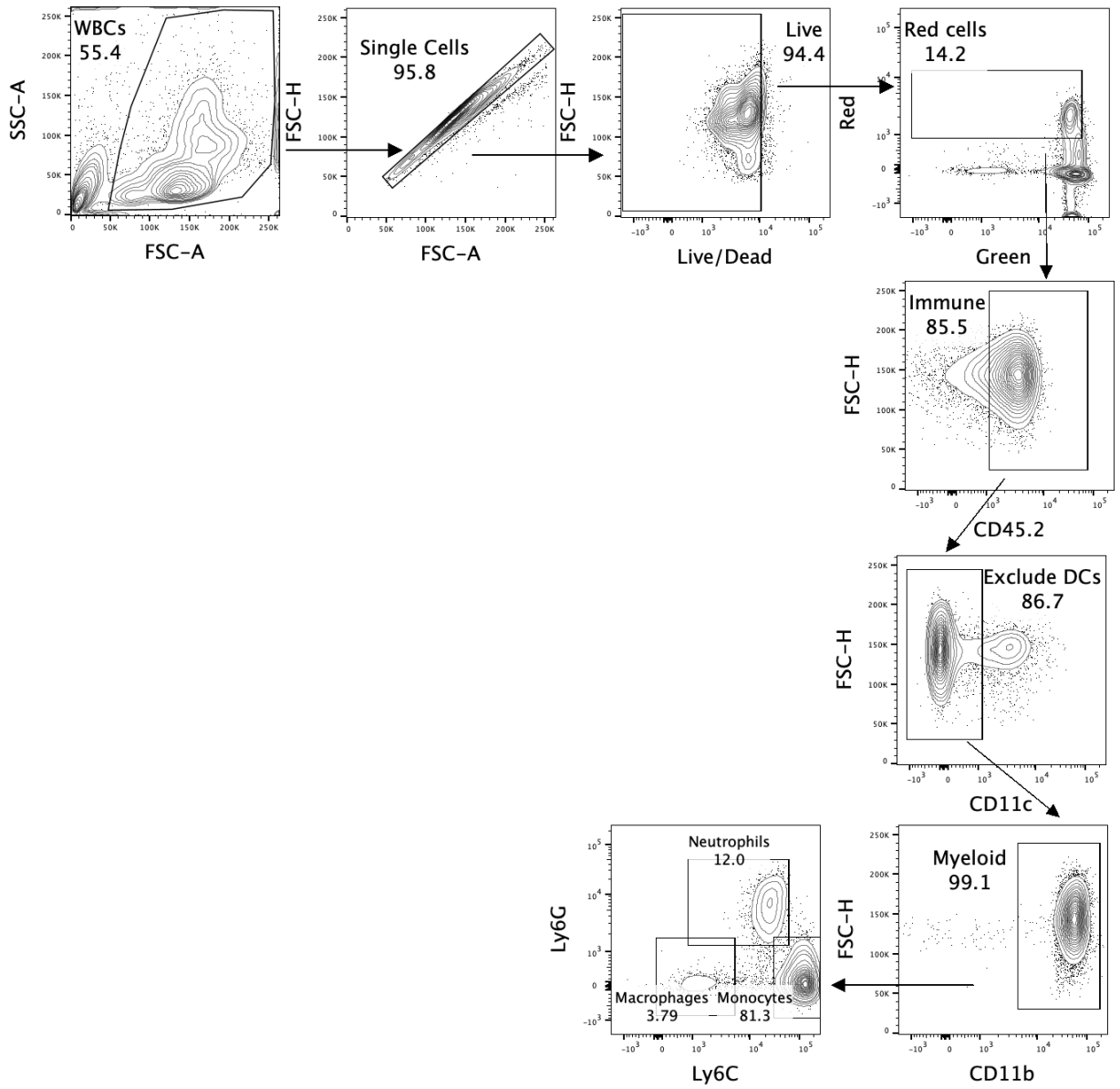

Figure 7

Flow cytometry gating scheme for mouse liver's innate immune cell populations on day 7 p.i. More concentrated circle = higher density of cells. The first plot (top left) identifies white blood

cells (WBCs) based on their characteristic forward and side scatter, showing a 55.4% presence. Moving right, the next plot ensures that the sample contains single cells (95.8%) by comparing forward scatter width and height, which helps exclude cell aggregates. The third plot distinguishes live (94.4%) from dead based on their differential uptake of viability dyes or scatter profile. The last plot in the top row selects red cells (14.2%) based on their emitted red fluorescence. Moving down, the first plot in the second row shows CD45+ cells (85.5%), a common leukocyte marker, indicative of a general immune cell population. Following the arrow, the next plot excludes DCs by gating on CD11c- population (86.7%). Going down, the next plot displays myeloid cells (99.1%), identified by their expression of CD11b, and the final plot to the left segregates neutrophils (12.0%), monocytes (81.3%), and macrophages (3.79%) based on the differential expression of Ly6C and Ly6G.

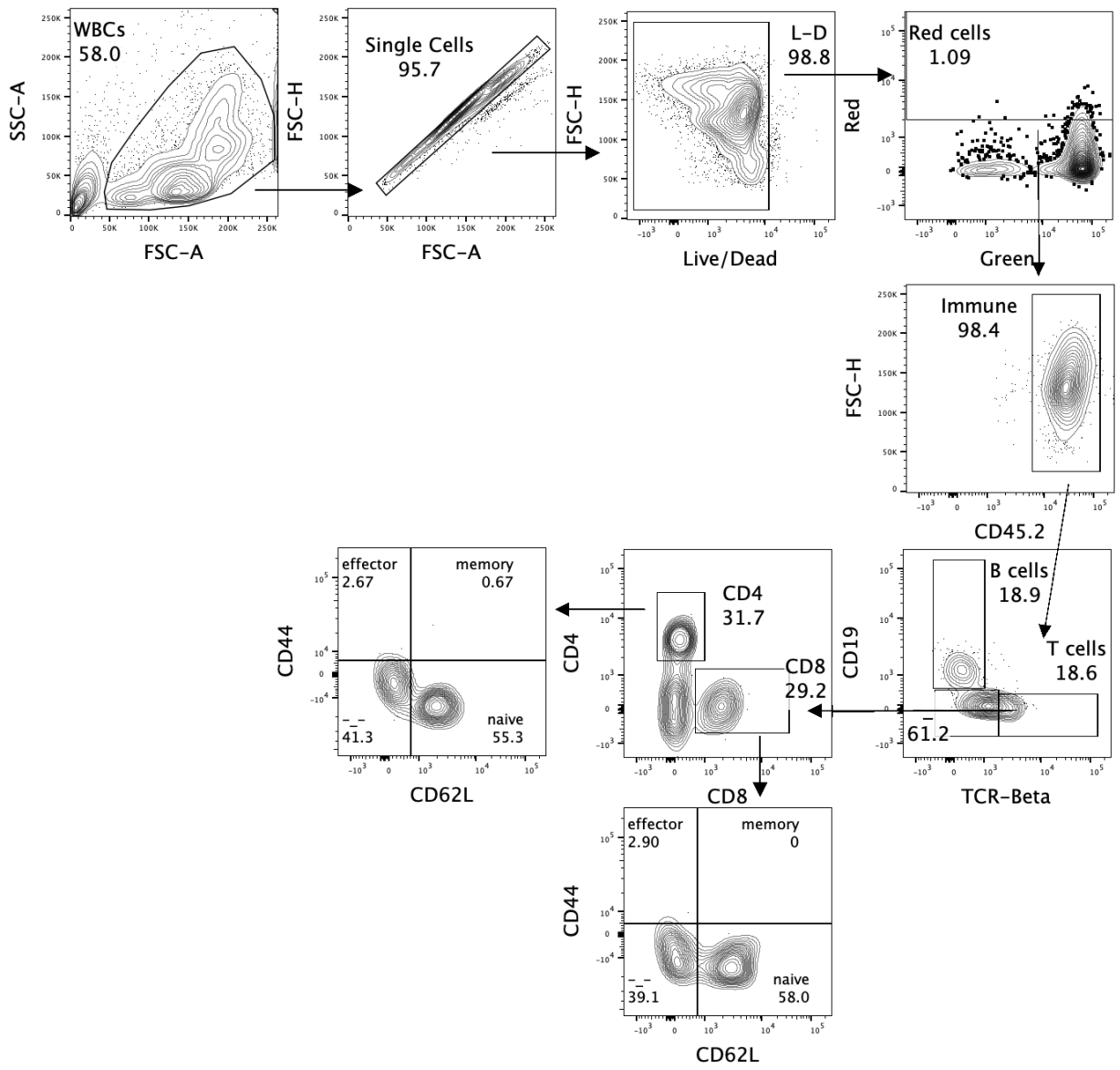

Figure 8

Flow cytometry gating scheme for mouse liver's adaptive immune cell populations on day 7 p.i. More concentrated circle = higher density of cells. The plots in the top row, like Figure 7, identify WBCs, single cells, live cells, and red cells, respectively. Going down from the red cells, the plot shows a nearly homogeneous population of CD45+ cells (98.4%), indicating that the vast majority of the cells in the sample are immune cells. Following the arrow, the next plot differentiates B cells (18.9%) from T cells (18.6%) using CD19 and TCR-Beta markers, respectively. Going left from the T cells, the plot distinguishes CD4+ helper T cells (31.7%) from CD8+ cytotoxic T cells (29.2%), both essential for orchestrating and executing immune responses. The CD4+ and CD8+ T cells are further characterized by the distribution of their subsets into naïve, memory, and effector cells,

which represent different stages of T cell activation and response. The majority of CD4+ and CD8+ T cells are naïve cells.

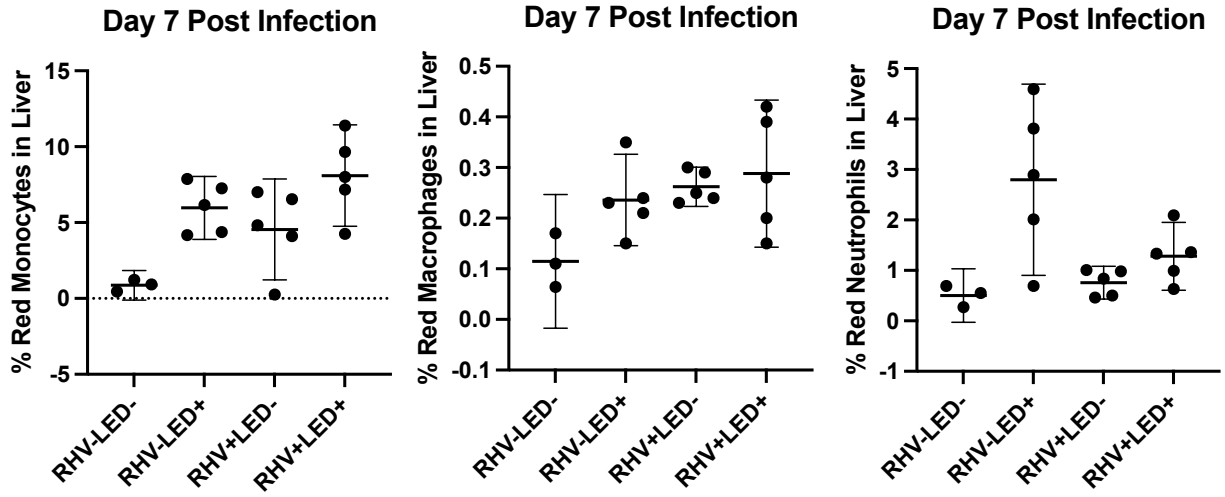

Figure 9

Percentage of red monocytes, macrophages, and neutrophils in the liver of infected vs. uninfected mice on day 7 p.i. (non-surgical groups included; the horizontal bold lines represent the means; the upper and lower error bars represent the 95% confidence interval)

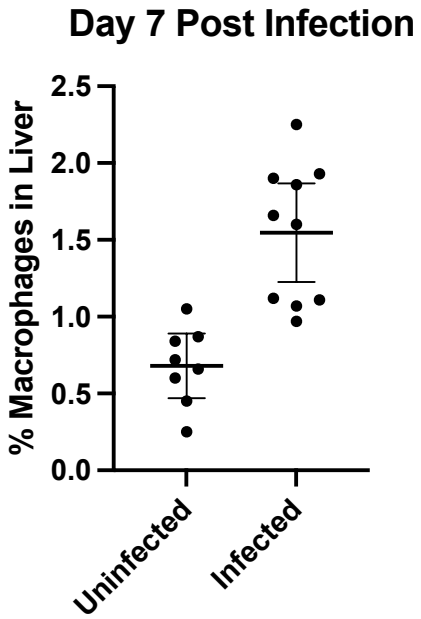

Figure 10

Percentage of liver-resident macrophages in the liver of infected vs. uninfected mice on day 7 p.i. (the horizontal bold lines represent the means; the upper and lower error bars represent the 95% confidence interval)

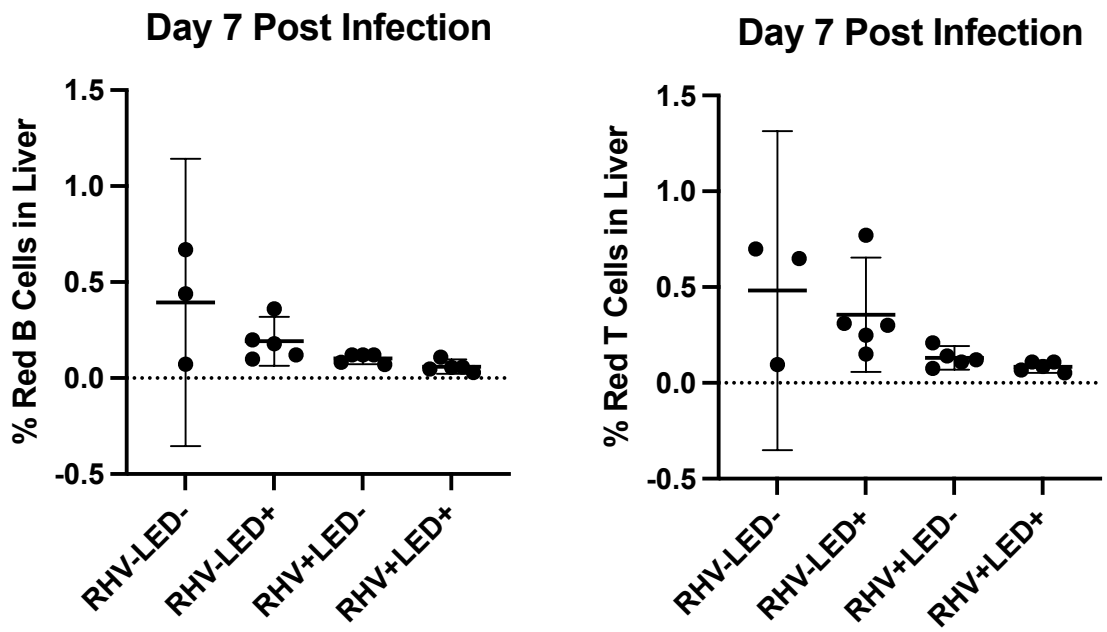

Figure 11
Percentage of red B cells and CD3 T cells in the liver of infected vs. uninfected mice on day 7 p.i. (non-surgical groups included; the horizontal bold lines represent the means; the upper and lower error bars represent the 95% confidence interval)

3. CCR2 Knock-out Mice Data

The presence of red macrophages and monocytes in the livers of infected mice on day 3 and 7 p.i. prompted an investigation of their roles. To address this, ten mice—five wildtype (WT) and five CCR2 knockout ($CCR2^{-/-}$) mice—were infected with RHV. They were then bled once per week for four weeks. Viral RNA was isolated from the serum and quantified using RT-PCR. The results showed that the viral load in each week was comparable between WT and $CCR2^{-/-}$, with only a few outliers observed. Additionally, by week four post-infection, most mice were on the verge of clearing the virus (**Figure 12**).

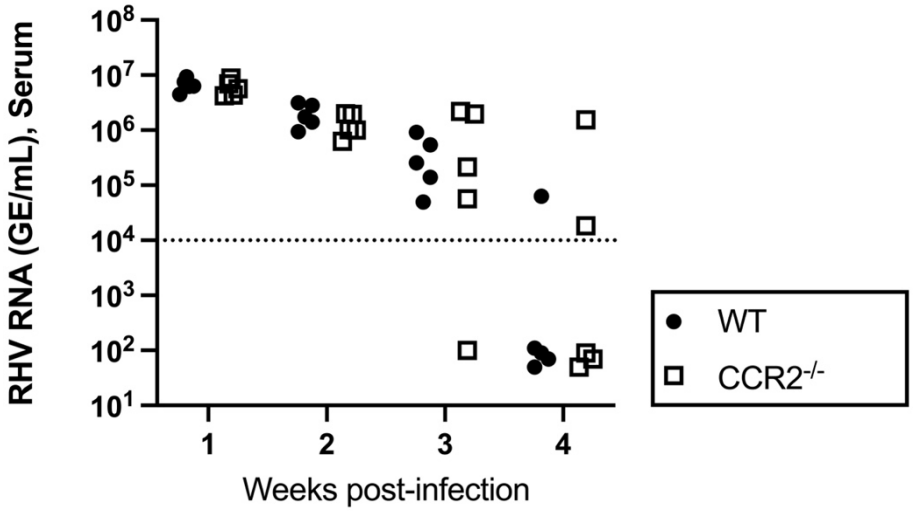

Figure 12
Comparison of serum RHV RNA levels (GE/mL) of WT and CCR2$^{-/-}$ mice 1-, 2-, 3-, and 4-weeks post-infection

4. Day 12 Post Infection

On the twelfth day p.i., there was a remarkable increase in the total number of cells and red cells in the liver of the infected mice compared to day 3 and 7 p.i.. Upon cell counting, the liver cells in the infected group were approximately six times more abundant than those in the uninfected group. Examination of the red cells in the liver showed an exclusive presence of adaptive immune cells, with no presence of innate immune cells like macrophages, monocytes, or neutrophils (**Figure 13 and 14**). There was a noticeable increase in the count of red B cells in the livers of the infected mice, which was almost statistically higher than that in the livers of the uninfected mice (**Figure 15**). Nonetheless, very few of these red B cells were plasma cells (**Figure 14**). Similarly, an even greater number of red T cells were found in the livers of the infected mice compared to the uninfected mice, with a statistically significant difference as indicated by the non-overlapping confidence intervals (**Figure 15**). Further analysis of the red T cell

subpopulations revealed that $CD4^+$ cells outnumbered $CD8^+$ cells by almost two-fold, predominantly consisting of effector cells. Interestingly, an increase in the number of $CD8^+$ memory cells was also observed (**Figure 14**).

The experiment conducted on day 12 p.i. was repeated. Again, the average number of liver cells in the infected group was approximately six times higher than that in the uninfected group. The red liver cells still remained devoid of any innate immune cells, although a very small, nearly negligible fraction consisted of red macrophages (**Figure 16 and 17**). Similar to the first trial, there was a significant increase in the number of red B cells and T cells in the livers of the infected mice, statistically surpassing those in the livers of the uninfected mice, as indicated by the non-overlapping confidence intervals (**Figure 18**), but still, very few of these red B cells were plasma cells (**Figure 17**). However, unlike the first trial, the red T cells comprised an equal proportion of $CD4^+$ and $CD8^+$ cells, with the majority still being the effector cells. The data also confirmed the presence of rising $CD8^+$ memory cells observed in the first trial (**Figure 17**).

A total of three experiments were conducted on day 12 p.i., with findings consistently revealing that the proportion of CD8 T cells in the liver was markedly elevated in the infected group compared to the uninfected group, with a statistical significant difference as indicated by the non-overlapping confidence intervals (**Figure 19**). Furthermore, the CD8 T cells in the infected group were predominantly effector cells, whereas those in the uninfected group were mostly naive cells. Moreover, the proportion of CD4 T cells in the liver was similar between the infected and uninfected group.

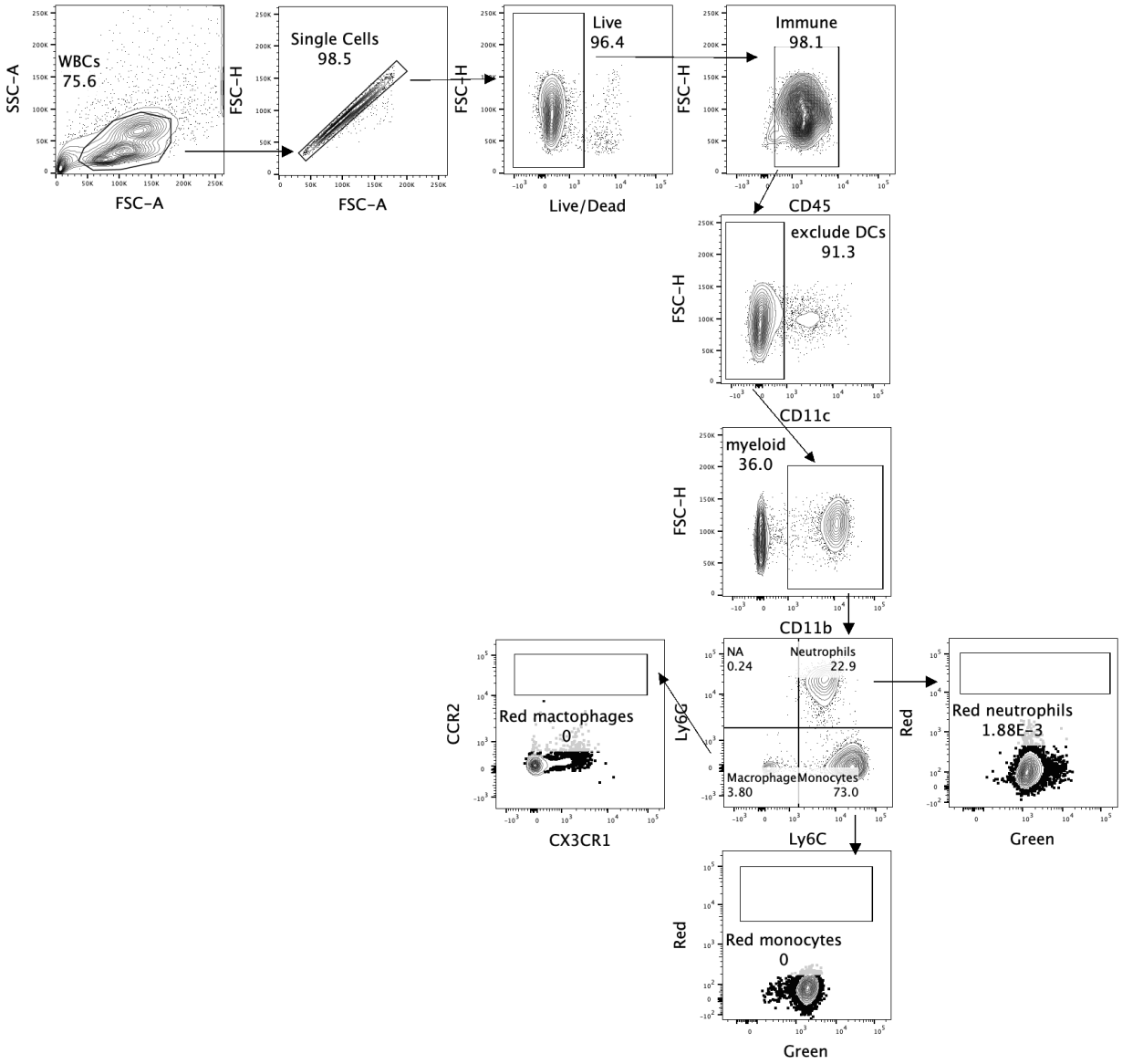

Figure 13

Flow cytometry gating scheme for mouse liver's innate immune cell populations on day 12 p.i. More concentrated circle = higher density of cells. The first plot (top left) identifies white blood cells (WBCs) based on their characteristic forward and side scatter, showing a 75.6% presence. Moving right, the next plot ensures that the sample contains single cells (98.5%) by comparing forward scatter width and height, which helps exclude cell aggregates. The third plot distinguishes live (96.4%) from dead based on their differential uptake of viability dyes or scatter profile. The last plot in the top row shows CD45+ cells (98.1%), a common leukocyte marker, indicative of a general immune cell population. Going down, the next plot excludes DCs by gating on CD11c- population (91.3%). Following the arrow, the next plot displays myeloid cells (36.0%),

identified by their expression of CD11b. Going down, the next plot segregates neutrophils (22.9%), monocytes (73.0%), and macrophages (3.80%) based on the differential expression of Ly6C and Ly6G. Going left, the plot identifies red macrophages (0%) based on their emitted red fluorescence as wel as expression of CCR2. Going right, the plot identifies red neutrophils (1.88E-3%) based on their emitted red fluorescence. Going down, the plot identifies red monocytes (0%) based on their emitted red fluorescence.

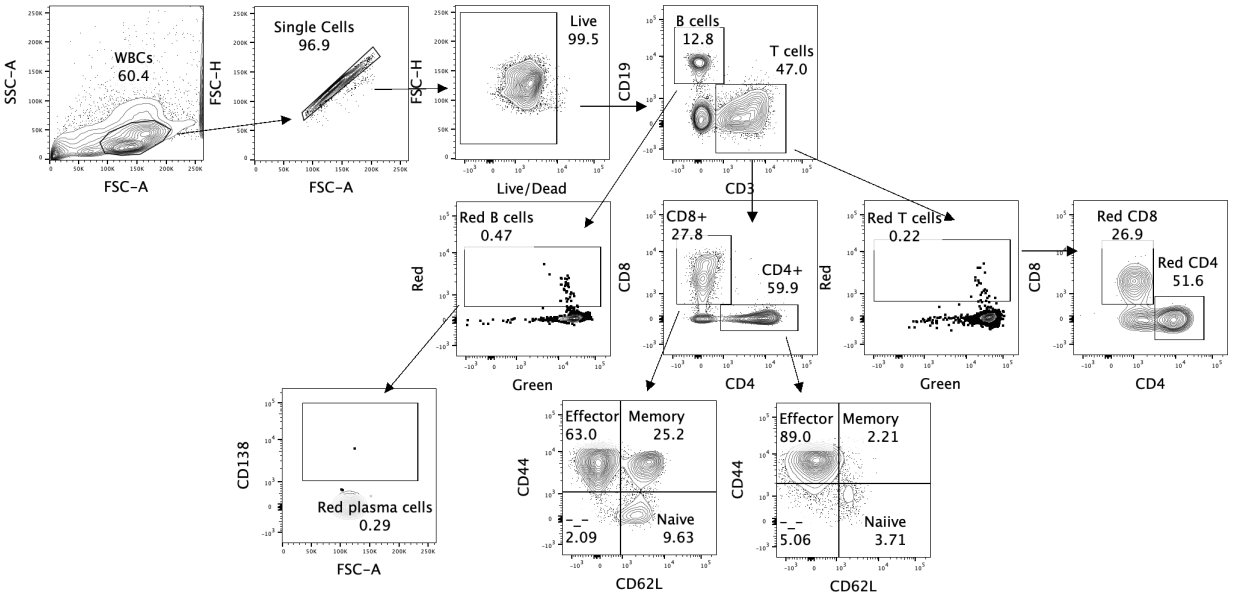

Figure 14

Flow cytometry gating scheme for mouse liver's adaptive immune cell populations on day 12 p.i. More concentrated circle = higher density of cells. The first plot (top left) identifies white blood cells (WBCs) based on their characteristic forward and side scatter, showing a 60.4% presence. Moving right, the next plot ensures that the sample contains single cells (96.9%) by comparing forward scatter width and height, which helps exclude cell aggregates. The third plot distinguishes live (99.5%) from dead based on their differential uptake of viability dyes or scatter profile. The last plot in the top row differentiates B cells (12.8%) from T cells (47.0%) using CD19 and CD3 markers, respectively. Going down from the B cells, the plot to left identifies red B cells (0.47%) based on their emitted red fluorescence. Following the arrow, the next plot identifies red plasma cells based on their expression of CD138. Going down from the T cells, the plot distinguishes CD4+ helper T cells (59.9%) from CD8+ cytotoxic T cells (27.8%), both essential for orchestrating and executing immune responses. The CD4+ and CD8+ T cells are further characterized by the distribution of their subsets into naïve, memory, and effector cells, which represent different stages of T cell activation and response. The majority of CD4+ and CD8+ T cells are effector cells, and one-fourth of CD8+ T cells are memory cells. Again, going down from the T cells, the plot to the right identifies red T cells (0.22%) based on their emitted fluorescence. Following the arrow to the right, the plot distinguishes red CD4+ (51.6%) from red CD8+ (26.9%).

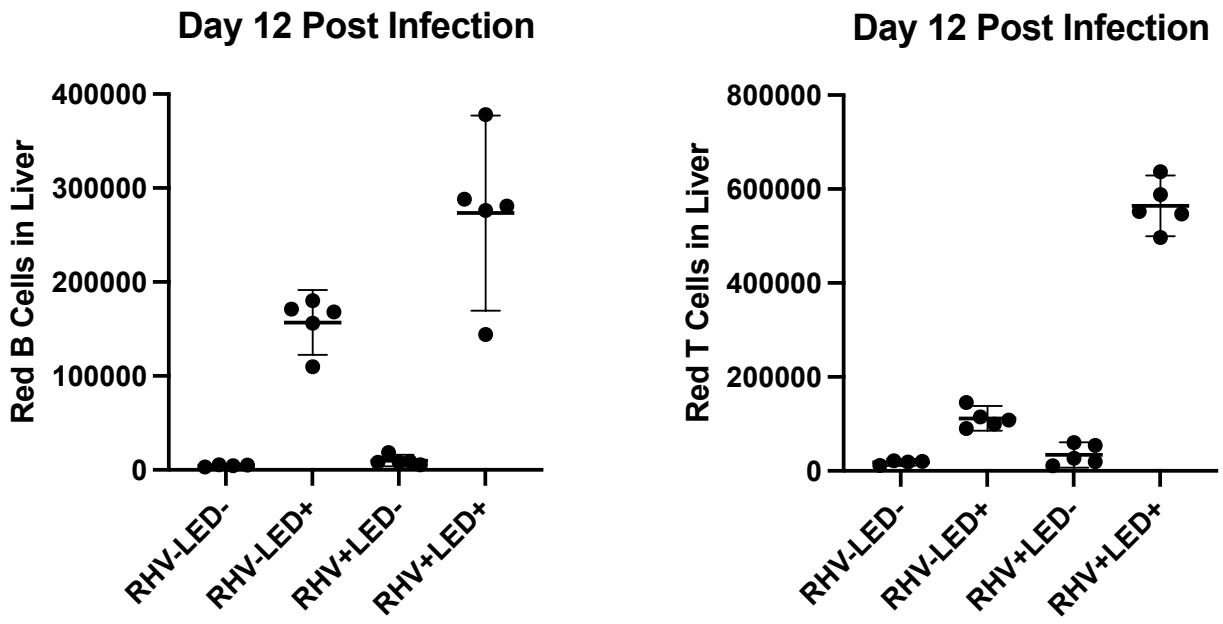

Figure 15

Total count of red B cells and CD3 T cells in the liver of infected vs. uninfected mice on day 12 p.i. (non-surgical groups included; the horizontal bold lines represent the means; the upper and lower error bars represent the 95% confidence interval)

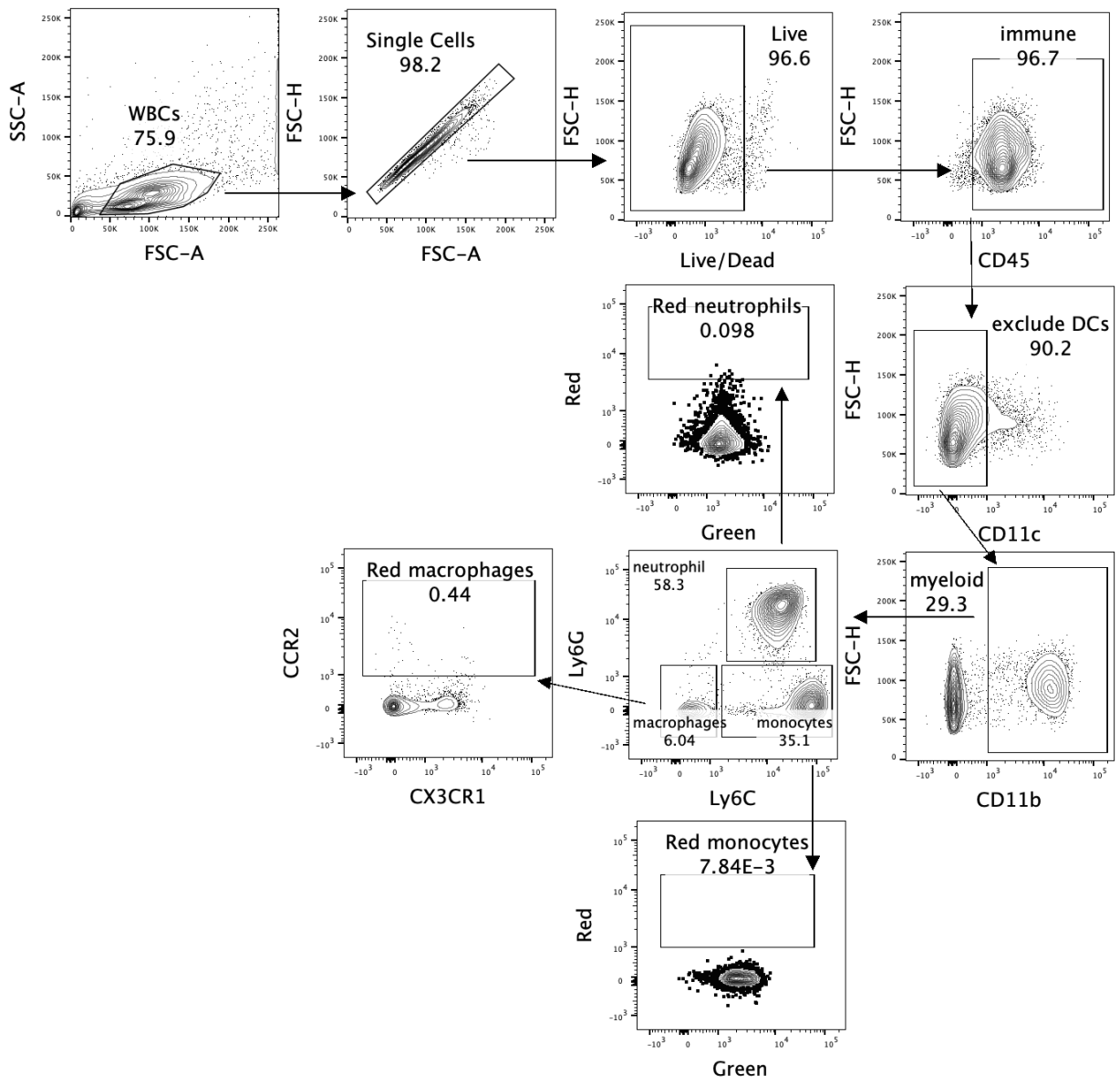

Figure 16

Flow cytometry gating scheme for mouse liver's innate immune cell populations on day 12 p.i.- repeat. More concentrated circle = higher density of cells. This is the same gating scheme as the one shown in Figure 13.

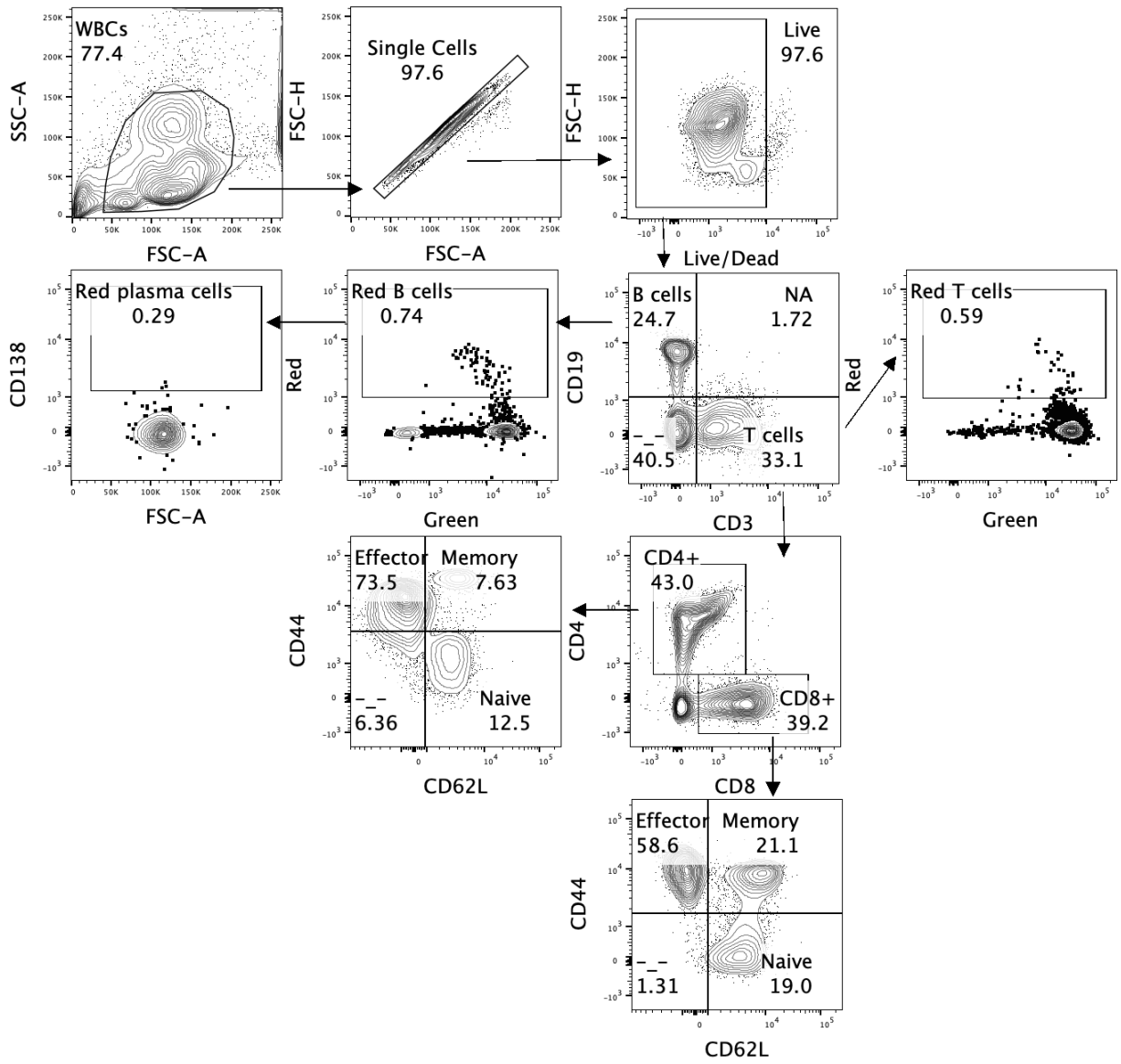

Figure 17

Flow cytometry gating scheme for mouse liver's adaptive immune cell populations on day 12 p.i.- repeat. More concentrated circle = higher density of cells. This is the same gating scheme as the one shown in Figure 14.

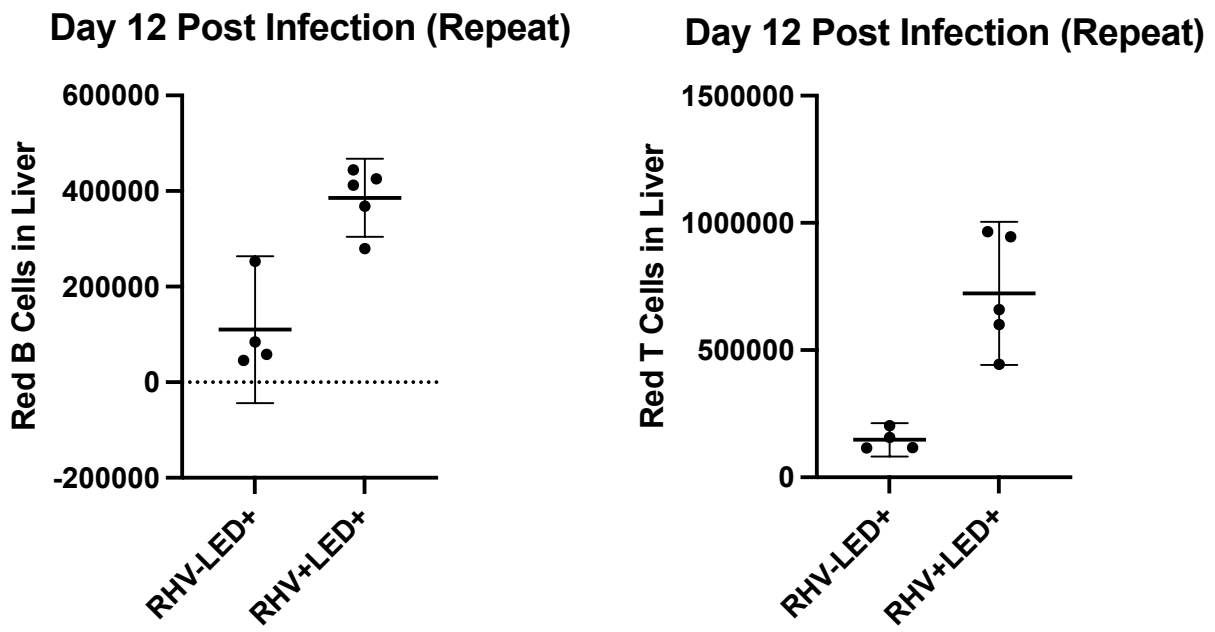

Figure 18

Total count of red B cells and CD3 T cells in the liver of infected vs. uninfected mice on day 12 p.i.-repeat (the horizontal bold lines represent the means; the upper and lower error bars represent the 95% confidence interval)

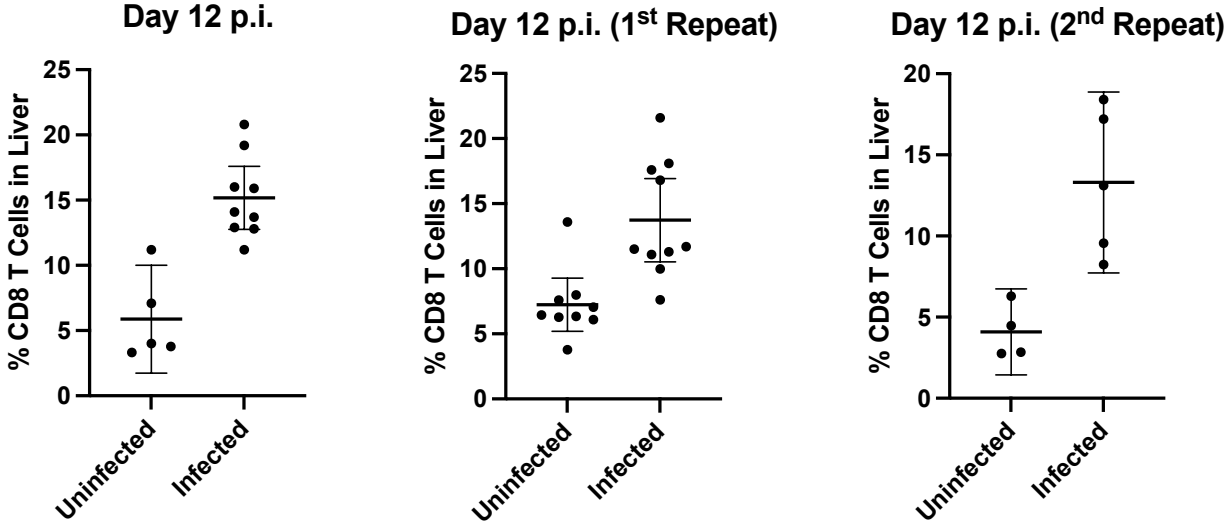

Figure 19

Percentage of liver-resident CD8 T cells in the liver of infected vs. uninfected mice on day 12 p.i. (the horizontal bold lines represent the means; the upper and lower error bars represent the 95% confidence interval)

4. DISCUSSION

The aim of this study is to assess the frequency and composition of cells migrating from the spleen to the liver during an acute RHV infection. Throughout the disease progression, it became evident that the virus prompted a gradual increase in liver cell proliferation, with a portion originating from the spleen.

On day 3 p.i., an early phase of the infection, we observed that some splenic cells had migrated to the liver in infected mice, exceeding those in uninfected mice. Analysis revealed a higher mean percentages of red neutrophils, red monocytes, and red dendritic cells in the liver of the infected mice compared to the uninfected mice, indicating the activation of the innate immune system to fulfill its role as the primary defense against the virus. The frequency differences among these cell types also corresponded well with the timeline of immune response. Neutrophils, being highly mobile, were the most abundant, reflecting their role as the earliest responders. Monocytes, which respond more slowly, were consequently less frequent, and macrophages, derived from monocytes, were expectedly least frequent. Dendritic cells, which link to the initiation of the adaptive immune system, remained at low levels, as anticipated. Interestingly, natural killer cells were not detected by flow cytometry, suggesting either their absence at this stage or difficulty in staining in the flow cytometry process.

The higher percentage of liver resident monocytes among all liver cells in the infected group compared to the uninfected group also implied an active role of the innate immune system during this period.

At this early time point, the adaptive immune system was expected to remain relatively inactive, supported by the nearly identical percentages of red B cells in the livers of infected and

uninfected mice. Although there seemed to be a migration of B cells from the spleen to the liver, it was unlikely these cells were viral-specific. However, the higher mean percentages of red T cells in the liver of the infected mice compared to the uninfected mice seemed to suggest some involvement of adaptive immune cells, but the low percentages of both $CD4^+$ and $CD8^+$ among these T cells suggested the opposite.

By day 7 p.i., an increase in the total number of liver cells was observed in the livers of infected mice compared to uninfected mice, as suggested by the observed larger cell pellet during tissue processing. Unlike day 3 p.i., there was a significant surge in the mean percentage of red monocytes in the liver of the infected mice, accompanied by a slight rise in the mean percentage of red macrophages. While these means were higher in the infected group, a larger sample size will be necessary for making definitive statistical conclusions. Nonetheless, this hinted at heightened mobilization of the innate immune response to combat the virus. Interestingly, the mean percentage of red neutrophils was lower in the liver of the infected compared to the uninfected. This could suggest neutrophil depletion at this stage, or perhaps their functions were assumed by monocytes and macrophages, leading to a decrease in their proportion. Same as day 3 p.i., no natural killer cells were detected, with the reasons remaining consistent with those mentioned earlier.

The elevated proportion of liver resident macrophages within all liver cells in the infected group, as opposed to the uninfected group, also indicated an active engagement of the innate immune system during this timeframe.

By this time, the adaptive immune system should start to function, but the statistics suggested otherwise. The percentages of red B cells and T cells in the liver remained low across

all groups, and this could mean that the B cells and T cells that naturally reside in the liver are participating in the immune response at this time. For the minuscule number of T cells that did migrate from spleen to liver as well as those local T cell population, they were consisted of nearly identical levels of $CD4^+$ and $CD8^+$ T cells. However, the majority of these cells were still in their naïve state, indicating their inactivity. This further supported the notion that the migration of the adaptive immune system remained relatively quiescent at this juncture.

It was anticipated that only mice in the surgical groups would exhibit the presence of red cells. However, flow cytometry data from day 7 p.i. revealed that mice in several non-surgical groups, especially the final control group, also displayed red cells in the liver. This irregularity may plausibly stem from exposure of cells to intense light at the stages of tissue processing and staining, inadvertently transforming the cells from green to red. To avoid this issue, subsequent experiments were meticulously carried out in environments with dim light or darkness.

This issue of bright light exposure might also impacted the data for day 3 p.i. experiment, although it was not manifested in the data since day 3 p.i. experiment did not include the non-surgical groups as controls. If it did impact the data, it would be unsure whether the red cells observed in the liver were splenic populations or liver resident populations.

It should be emphasized that for experiments conducted on day 3 and 7 p.i., a precise count of cell numbers was not obtained due to the design of the protocol. Given that day 3 p.i. represents an early stage of the infection that does not result in a marked increase in liver cell numbers, the percentages obtained could be meaningful within this specific context. Nonetheless, by day 7 p.i., an escalation in liver cell numbers is anticipated and was actually observed in the infected group, rendering the percentage-based comparisons potentially

imprecise. Consequently, the conclusions drawn for day 7 p.i. necessitate a reassessment in light of the variance in cell counts. It is possible that both the innate and adaptive immune responses were notably active during this period.

The discovery of red macrophages and monocytes in the livers of infected mice on day 3 and 7 prompted an investigation into their potential roles in disease progression and viral clearance. To explore this further, five wildtype (WT) and five CCR2 knockout ($CCR2^{-/-}$) mice, lacking CCR2 production, were infected with RHV and bled weekly for four weeks to quantify their viral RNA levels. Comparing viral loads between the two groups over the four-week period revealed no significant difference. Both $CCR2^{-/-}$ and WT mice showed similar mean viral loads in each week, with both groups nearing viral clearance by the fourth week. These findings collectively suggested that $CCR2^{+}$ monocytes/macrophages were unlikely to play a role in RHV progression and clearance. Consequently, the presence of these cells in the livers of infected mice on day 3 and 7 post-infection might not be specific to viral infection.

On day 12 p.i., the observation of a higher number of liver cells in the infected group was a promising result. The red liver cells, however, were made up of adaptive immune cells exclusively. The absence of red innate immune cells and the presence of red adaptive immune cells were supposed to be the expected results for day 12 p.i. Red B cells were higher in total number in the liver of the infected compared to the uninfected, yet very few of these B cells were plasma cells- essential for viral clearance, either because they had not differentiated yet or because they would not become plasma cells after all. Moreover, existing literature suggests that staining and tracing plasma cells can be particularly challenging (Kumar et al., 2023). Red T cells, similarly, were discovered to be in elevated amount in the liver of the infected compared to the uninfected.

These red T cells were composed of $CD4^+$ and $CD8^+$, with $CD4^+$ two time more than $CD8^+$. The majority of these cells were still effector cells, and interestingly, some $CD8^+$ had developed into memory cells. Collectively, these results offered a holistic picture of an ongoing adaptive immune system.

The results of the repeated experiment for day 12 p.i. closely mirrored those of the first trial, reinforcing the activity of the adaptive immune system while negating that of the innate immune system on day 12 p.i..

Additionally, the three day 12 p.i. experiments consistently illustrated a significant increase in the proportion of CD8 T cells within the liver of the infected group compared to the uninfected group. Moreover, the CD8 T cells within the infected group were largely comprised of effector cells, contrasting with the predominance of naive cells in the uninfected group. These findings implied robust activity of the adaptive immune system within the liver on day 12 p.i..

In the ongoing study, attention will shift to the dynamics of immune cell activity on day 14, 21, and up to week 4 p.i.. The study will primarily investigate the formation of plasma cells in the liver, their migration to various tissues, and their ultimate relocation to the bone marrow. With the inclusion of this additional data, a complete picture of the immune activity during RHV infection can be drawn.

5. CONCLUSIONS

The study offered an in-depth examination of the immune response dynamics during an acute RHV infection. Combining an innovative methodology with flow cytometry, the study explored the roles and kinetics of various immune cells, offering insights into the complexities of RHV

infection and contributing to a broader understanding of HCV pathogenesis and immune responses.

The study unveiled a complex interplay between the body's innate and adaptive immune response throughout various stages of RHV infection. In the early phase (day 3 p.i.), although the conclusion that there was a notable migration of immune cells, predominantly neutrophils, monocytes, and dendritic cells, from the spleen to the liver might be complicated by the stated artifact of bright light exposure, further observation of a higher percentage of liver-resident monocytes in the infected group compared to the uninfected group still indicated an immediate activation of the innate immune system in the liver.

As the infection proceeded to the early to mid-phase (day 7 p.i.), there was a notable rise in the emergence of local macrophages in the liver, signifying a heightened innate immune response. Conversely, the quantities of splenic B cells and T cells in the liver were comparatively small, suggesting a potentially postponed or more regulated activation of the adaptive immune system. This was also supported by liver-resident B cells and T cells staying in their inactivated, naive state.

On day 12 p.i., there was a notable migration of B cells and T cells from the spleen to the liver, and the liver's immunity was dominated by effector T cells, a sign of engagement from the adaptive immune system. Especially, there was a significant rise in liver resident $CD8^+$ effector cells, heralding a shift towards a more robust adaptive immune response. Another significant observation was the development of $CD8^+$ memory cells, suggesting an evolving maturity within the adaptive immune system.

All in all, the study concluded that both innate and adaptive immune responses played pivotal roles in the course of RHV infection. The findings emphasized the importance of migratory innate immune cells and liver-resident monocytes and macrophages in the early immune response, while the adaptive immune response, particularly the activation and proliferation of liver-resident $CD8^+$ T cells as well as those migratory B cells and T cells, was crucial in the later stages. These insights not only enhanced the understanding of RHV pathogenesis but also contributed valuable knowledge to the broader field of viral infections and immunity, potentially informing future research and therapeutic strategies against HCV and other similar viral infections.

The successful implementation of KiKGR ROSA26 knock-in mice in this study opened up new possibilities in related research. Despite challenges of tissue identification and labeling, this approach enables the comparison of various viruses' mechanisms. Given the vital roles of immune cell circulation in establishing immunity, the insights gained from the research could have significant implications for vaccine developments.

6. REFERENCES

Alter, Miriam J. "Epidemiology of hepatitis C virus infection." *World journal of gastroenterology: WJG* 13.17 (2007): 2436.

Atcheson, Erwan, et al. "Use of an outbred rat hepacivirus challenge model for design and evaluation of efficacy of different immunization strategies for hepatitis C virus." *Hepatology* 71.3 (2020): 794-807.

Billerbeck, Eva, et al. "Mouse models of acute and chronic hepacivirus infection." *Science* 357.6347 (2017): 204-208.

Bronte, Vincenzo, and Mikael J. Pittet. "The spleen in local and systemic regulation of immunity." *Immunity* 39.5 (2013): 806-818.

Chen, Stephen L., and Timothy R. Morgan. "The natural history of hepatitis C virus (HCV) infection." *International journal of medical sciences* 3.2 (2006): 47.

Hartlage, A. S., et al. "Vaccination to prevent T cell subversion can protect against persistent hepacivirus infection." *Nat Commun*. 10.1 (2019): 1113.

Hayes, C. Nelson, et al. "Road to elimination of HCV: Clinical challenges in HCV management." *Liver international* 42.9 (2022): 1935-1944.

Kapoor, Amit, et al. "Identification of rodent homologs of hepatitis C virus and pegiviruses." *MBio* 4.2 (2013): 10-1128.

Kumar, Deepak, et al. "An alternative processing approach to increase CD138 intensity in flow cytometric analysis of plasma cells." *Cytometry Part B: Clinical Cytometry* (2023).

Li, Haijun, and Zhengkun Tu. "The Role of Monocytes/Macrophages in HBV and HCV Infection." *Biology of Myelomonocytic Cells* (2017).

Mueller, Scott N., and Barry T. Rouse. "Immune responses to viruses." *Clinical Immunology* (2008): 421.